The effect of Pore Connectivity on Mercury Entrapment

Nuradeen Labaran Tanko

Abstract— In recent decades, Mercury Entrapment has beeen stated to depend on geometric properties of porous materials such the Pore Size Distribution, Pore Size, Shape, Connectivity, Porosity and many more. However, there is no work in the literature to show a clear relationship between topologigcal properties such as the Pore Connectivity and Mercury Entrapment. In this work, a simple geometry correlation for Connectivity of flow path and porosity in porous media is presented. The materials studied are chemically pure mesoporous silica and alumina catalyst support pellets with simplified pore sizes, pore side dsitribution, and surface Chemistry. The Pore Connectivity of the samples are estimated with the aid of Percolation theory using a standard technique of Gas Sorption and the enrapment from retraction curves of mercury porosimetry. In conclusion, despite the limitations of the pore connectivity descriptor a trend exits to support the hypothesis that Mercury Entrapment increases with a decrese in Pore Connectivity. However, after careful analytical consideration, the correlation obtained between the two characteristic parameters are ruled to be signifant. Nevertheless, this the trend is established.

Index Terms - Porous Media, Mercury Porosimetry, Mercury Entrapment, Gas Adsorption Porosimetry, and Pore Connectivity

1 INTRODUCTION

The size, shape, and arrangement of conducting spaces in porous materials, such as reservoir rocks, are known to affect the flow of fluids and the displacement of one fluid by another [1,2]. Pores and throats of different sizes may be distributed randomly in a network (randomly heterogeneous) or they may be distributed non-randomly [3]. In the latter case, the larger elements may be clustered together in domains and likewise the smaller elements are clustered together in other domains. In Mercury porosimetry, the wetting fluid preferentially saturates larger pores upon pressure increase but the opposite happens when pressure is reduced as the smaller pores empty in a uniform manner. Therefore, at the completion of intrusion-extrusion cycle, the retraction curve does not give zero volume, and thus some of the mercury is entrapped [4].

One of the earliest studies aimed at explaining the origin of hysteresis and entrapment was conducted by [5] with the aid of two-dimensional network model consisting of cylindrical pore segments assembled into square grids. These workers found that entrapment increased as the pore size distribution got wider, and that the mercury was preferentially entrapped in larger pores. Thus, this finding suggests that mercury retraction might involve a slower relaxation process as well as the more rapid, capillary flow process described by [6]. The workers attributed this slow retraction process to the formation of ganglia of entrapped mercury that, under a non-zero net force prior to equilibration, tends to move around slowly and may coalesce with the bulk. Therefore, it might be inaccurate to interpret mercury retraction solely on the basis of a piston-like withdrawal. Similarly, [7,8] conducted a mercury porosimetry on model porous media consisting of various different types of pore networks etched in glass. The mercury porosimetry experiments, conducted by these researchers suggested that non-random structural heterogeneity causes mercury entrapment which was in good agreement with subsequent experimental work of [9] on glass micromodels.

In a different approach, a three-dimensional pore bond network modelling approach was adopted by [10] to investigate the effects of pore size distribution and pore connectivity from the results of mercury porosimetry experiments. The inherent flexibility of this model facilitated the construction of networks with varying connectivities or distributions of connectivities. The results from simulations of standard intrusion/extrusion cycle porosimetry experiments suggested that there was a characteristic entrapment of mercury for a network comprising a Gaussian pore size distribution. Furthermore, the researchers stated that entrapment is dependent on the pore connectivity, variance, $\frac{\sigma}{\mu}$, where σ is the standard deviation of the pore size distribution and μ is the mean pore size distribution. These findings are in good agreement with [5,6,11].

It is still unclear if the results from computer simulation and micromodels can explain the cause of hysteresis and mercury entrapment in amorphous porous media. The pore structures of amorphous materials, such as oil reservoir rocks and heterogeneous catalyst support pellets, are considerably more complex than the micromodels investigated by researchers [5,7,10,11]. It is in this regard that this paper further elucidates and expands the works of those researchers on a range of alumina and silica materials. The pore connectivity can be estimated by using Percolation theory.

Mercury porosimetry is probably still the only method by which a macroscopic porous material can be characterised using just a single technique. In principle, mercury porosimetry can be used to obtain the porosity, specific pore volume, pore connectivity [11], and the spatial distribution of pore size [12,13]. Despite the limitations addressed above, mercury porosimetry is widely used in characterisation of catalyst support pellets [14,15], cement based materials [16,17], granite and saprolite materials [18,19], and sedimentary rocks [1,20].

An analysis method, based on percolation theory, has been widely used for the determination of the connectivity of porous solids from hysteresis of nitrogen sorption measurements [21-24]. [25] best described the percolation theory and explained, that the square lattice can be considered to consist of a number of bonds that can either be occupied (denoted by a line) or unoccupied. In recent decades, [21] modelled the solid structure as an array of three-dimensional lattices with each lattice corresponding to the pore network of a microparticle. The researcher viewed the hysteresis between the adsorption and desorption isotherms as a percolation phenomenon. Thus, the sharp decrease in the amount adsorbed at the knee of the desorption isotherms corresponds with the formation of a percolating network of vapour-filled pores. It was suggested by [21], that a percolation cluster of pores, which are below their condensation pressures, is formed, and the metastable liquid nitrogen in these pores vaporises. Also, as the pressure drops further, f (percolation factor) increases and the nitrogen in the rest of the pores vaporizes. Consequently, [21] concluded that, the primary desorption is a connectivity related phenomenon that can be described by percolation theory. This

theory is based on the connected structures formed by random links on a lattice. The classical percolation theory focuses on two main problems, the bond percolation problem, and the site percolation problem. In closure, the pore size distribution is one of the most important requirements for predicting diffusivity and entrapment. In addition, mercury entrapment is strongly dependent on the topological properties of porous media. The effect of tortusotity on mercury entrapment was investigated by experimental and simulation [26-29]. Also, there are other simulation works that suggest tortuosity for molecular diffusion increases with decreasing pore connectivity, and increasing width of PSD by [30-34]. Therefore, based on these simulations, it is safe to conclude that a correlation exists between mercury entrapment and pore connectivity since they both depend on the same network parameters.

2 THEORY

Mercury porosimetry can give information that is valuable in assessing multiphase fluid behaviour of oil and gas in a strongly water-wetting system and the trapping of oil or gas that is controlled mostly by capillary forces, and thus, a direct analogy with the air-mercury system is possible [38]. It is in this regard that this study adopts Mercury porosimetry for the samples under investigation. In mercury porosimetry, the Laplace equation, also known as the Washburn equation, can be employed to relate an applied pressure with a relevant pore diameter being intruded by the non-wetting liquid mercury.

$$\Delta p = \gamma_{HG}\left(\frac{1}{r_1}+\frac{1}{r_2}\right)=\frac{2\gamma_{HG}\cos\theta}{r_P} \tag{1.0}$$

The Washburn equation (Equation 1.0) relates the pressure difference across the curved mercury interface (r_1 and r_2 being the radii of curvature of that interface) to the corresponding pore size (r_p) using the surface tension of mercury (γ_{HG}) and the contact angle (θ) between the solid and mercury. The volume of mercury penetrating the pores is measured directly as a function of the applied pressure. According to [35], a value of 0.485 N/m at 25 °C is generally accepted for surface tension and a fixed value of 130° for the contact angle (irrespective of the sample material). However, the surface or interfacial tension of mercury contributes greatly with respect to errors in the determination of the pore size distribution and can change with pore size [35].

For the estimation of Pore connectivity, [21] method was adopted. That a percolation cluster of pores, which are below their condensation pressures, is formed, and the metastable liquid nitrogen in these pores vaporises. Thus, as the pressure drops further, f (percolation factor) increases and the nitrogen in the rest of the pores vaporizes. Consequently, [21] concluded that, the primary desorption is a connectivity related phenomenon that can be described by percolation theory. This theory is based on the connected structures formed by random links on a lattice. The classical percolation theory focuses on two main problems, the bond percolation problem, and the site percolation problem.

The primary adsorption process in the capillary condensation region can be treated as a classic site (cavity) percolation problem. Thus, desorption process for systems with hysteresis is the bond (connection) percolation problem. The value f which is the fraction of occupied bonds represents the number of occupied bonds divided by the total number of bonds. In addition, the worker defined the percolation probability (F) that a bond is part of the percolation cluster, and Z as coordination number. [21] used this analogy to further investigate the percolation theory, and their resulting representation is shown in Figure 1.0, where the percolation threshold for the lattice is 0.5.

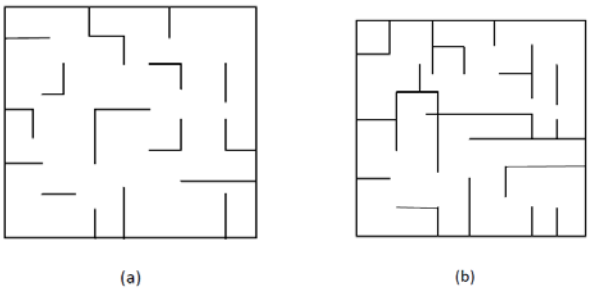

Figure 1.0
Percolation in a 2D lattice (a) f = 0.25, (b) f = 0.5, percolation threshold [21]

The near percolation threshold, which is the number of occupied bonds per site in the percolation cluster, ZF, is an approximately universal function of the mean number of occupied bonds per site Zf. The effect of system size on $F(f)$ is given by a modified finite-size scale scaling equation as:

$$L^{\frac{\beta}{\nu}} ZF = h\left[\left(Zf-\frac{3}{2}\right)L^{\frac{1}{\nu}}\right] \tag{2.0}$$

where the critical components, β and ν have values 0.41, and 0.88, respectively, in three dimensions. The scaling function, h, has the same general shape for all 3D systems which vary from lattice to lattice. Figure 2.0 illustrates the generalised scaling function.

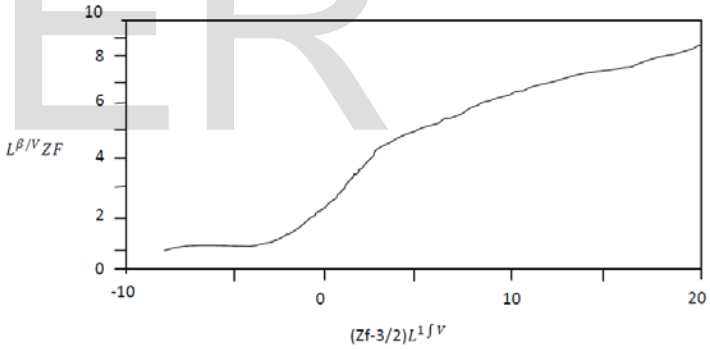

Figure 2.0
Illustration of the generalised scaling function [21]

$V_{Absorbed}$ **(cm³/g at STP)**

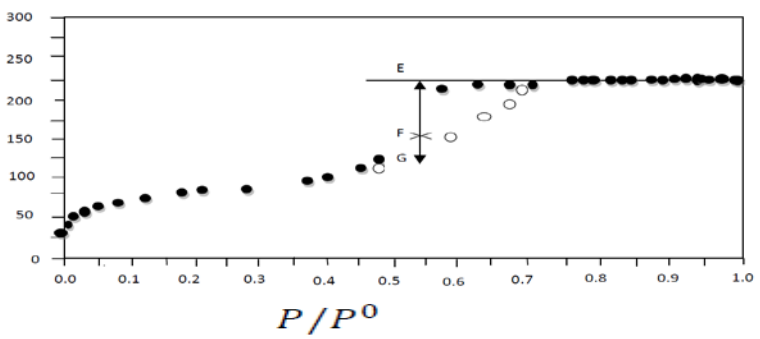

Figure 3.0

Schematic illustration of the calculation of $\frac{F}{f} = \frac{EF}{EG}$ **[21]**

The procedure for the determination of pore network connectivity involves three stages:

- The pore size distribution is determined by using the method of [25]. An appropriate pore shape must be assumed.
- $F(f)$ is determined from the adsorption and desorption data as illustrated in Figure 3.0.
- The size and shape of the hysteresis loop is dictated by the mean coordination number of the pore network, Z, and the number of pore lengths, L. The connectivity parameters, Z and L are obtained by fitting the quasi-universal curve of Equation 2.0 to $F(f)$.

2.3 Materials

The materials studied in this work are commercially available, chemically pure mesoporous silica and alumina catalyst support pellets with simplified pore sizes, pore size distribution, and surface chemistry. As highlighted in Table 1, the materials have pore size lying in the range of 7-30 nm. The majority of the materials have unimodal structure with the exception of one bimodal structured material (AL3984T).

Table 1.0
A range of alumina and Silica materials tested

S/N	Sample	Material	Pellet form	Voidage	Nominal diameter (mm)
1	Aerosil	Silica (SiO_2)	Fumed sphere	N/D[a*]	3.5
2	AL3984T	Alumina (Al_2O_3)	Tablet	0.59	3.0
3	AL3992E	Alumina (Al_2O_3)	Extrudate	0.65	3.0
4	C10	Silica (SiO_2)	Gel sphere	0.66	3.0
5	C30	Silica (SiO_2)	Gel sphere	0.69	3.0
6	P7129	Silica (SiO_2)	Gel sphere	0.67	3.0
7	Q17/6	Silica (SiO_2)	Gel sphere	0.49	3.5
8	S980A	Silica (SiO_2)	Gel sphere	0.6	3.0
9	S980G	Silica (SiO_2)	Gel sphere	0.61	2.2
10	Silica Alumina	Silica and Alumina (Al_2O_5Si)	Extrudate	0.60	0.5

Note: a* – Not detected

Dr. Nuradeen Labaran Tanko, Petroleum and Gas Engineering Department, Baze University, Abuja-FCT, Nigeria, Mobile No. +2348067664333. (e-mail: nuradeen.tanko@bazeuniversity.edu.ng).

2.4 Experimental Consideration

2.4.1 Gas Sorption Porosimetry

On each sample, nitrogen sorption experiment was carried out at 77K using a Micromeritics accelerated surface area porosimeter (ASAP) 2010 apparatus. Initially, about 0.2 g of the sample was left under vacuum for 4 hours at a pressure of 0.27 Pa as recommended by [36]. The purpose of the thermal pre-treatment for each sample was to drive any physisorbed water on the sample while leaving the morphology of the sample itself unchanged. The sample tube and its contents were then re-weighed after cooling to room temperature. Thus, the dry weight of the sample before being transferred to the analysis port for the automated analysis procedure was measured.

A full adsorption/desorption micro/mesoporous was carried out since the samples' characteristics were unknown. The calculation of the dead volume of flask (free space analysis) was carried out by using helium. The dead space was the volume of the sample tube excluding the sample itself. As also recommended by [36], equilibration time for the diffusion of nitrogen molecules to access most of the pores present in these materials was set
at forty five seconds.

In the Kelvin Equation $\left[RT \ln x = \frac{-2\gamma_{LV} V_L \cos\theta}{r_k} \right]$, the adsorbate property factor was taken as 9.53×10^{-10} m. Furthermore, it was assumed that, the fraction of pores open at both ends was zero, for both adsorption and desorption. Thus, capillary condensation commenced at the closed end of a pore to form a hemispherical meniscus, and the process of evaporation commenced at a hemispherical meniscus.

2.4.2 Mercury Porosimetry

The AutoPore III 9420 mercury porosimeter is designed to perform low pressure analysis of four samples at one time. The equipment is designed to perform two high pressure analyses at the same time. The equipment measures the intruded volume in relation to the mass of the sample at a specific pressure; this pressure can be converted to an equivalent Laplace diameter according to Washburn Equation $\left[\Delta P = \frac{2\gamma_{HG} \cos\theta}{r_p} \right]$. The amount of mercury intruded is determined by the fall in the level of the interface between the mercury and the compressing fluid. A value of 0.485 Nm^{-1} at 25 °C is generally accepted for surface tension and a fixed value of 130° for the contact angle, as a result, were adopted in this study. If less than four samples are to be analysed, a blank rod must be installed in the unused low pressure ports. Vacuum conditions cannot not be achieved if penetrometers or blank rods are not installed in an unused pressure port.

Porous materials are prone to adsorb water or other chemicals, and therefore the sample has to be cleared of these contaminants before the analysis by heating. The purpose of the thermal pre-treatment for each sample was to drive any physisorbed water on the sample leaving the morphology of the sample itself unchanged. A pre-treatment condition of 250 °C for 4 hours used by [36] was adopted for this study. A powder penetrometer (3cc powder) was used due to the small physical size of the materials. The weight of the empty sample flask was registered prior to introducing the sample. The sample (~ 0.7

g) was loaded into the penetrometer, which consisted of a sample cup connected to a metal-clad, precision-bore, and glass capillary stem. A vacuum tight seal (Apiezon H) was used to fill the inevitable roughness of the ground glass lip and polished surface. Care was taken when applying the grease as too much grease exposes the sample to an unwanted coating, whilst too little grease results in an imperfect seal. The penetrometers were sealed with spacers over the stem and placed in low pressure ports, where the sample was evacuated to remove air and moisture. The sample cell was evacuated and filled with mercury while the entire system was still under reduced pressure. The first data point was taken at a pressure of 3000 to 4000 Pa or higher. At the end of the low pressure analysis, the weight of the penetrometer filled with mercury and sample was determined. The measured value determines the bulk density of the sample by using corresponding blank-runs as a reference. Once the preweighed sample from the low pressure analyses port was transferred to the high pressure system, the sample and the injected mercury from the low pressure system was surrounded by hydraulic fluid and pressurised up to 414 MPa. Both chambers were tightly closed and had sufficient high pressure fluid drawn into the vent valve. If the fluid was above the visible ledge level, excess fresh fluid was removed to bring the level to the ledge.

In order to calculate the true volume intrusion of mercury into the pores of a sample, a correction was made to account for the compression of mercury, sample cell and sample. Compressibility (β^0) is the fractional change in volume per unit pressure change and therefore a major effect that has to be addressed [37]. Ideally, this problem can be corrected by a corresponding blank run using a non-porous sample of the same material. However, the blank run does not always solve the problem as encountered in the course of these experiments. One of the adjustments made was to create separate blank runs with the same respective equilibration time as those used in the experiments.

4 Result and Analysis

For gas adsorption analysis, in order to allow for the variation of support structure between pellets from the same batch and to test the reproducibility of measurements, replicate measurements are used. Sets 1 and 2 represent the replicate measurements, respectively. Therefore, the reported parameters in this section are the mean of the sets used. Also, during the course of experiments, the relative pressure was either increased or decreased in small steps, and a small volume of nitrogen, either enters, or leaves, the sample.

The connectivity estimations in Table 2.0 are carried out in terms of percolation variables as described in Section 2.0. These values are calculated from the PSD using the method of [38]. The hysteresis loop was used to determine the number fraction of pores that would have been emptied in a perfectly connected network, f, and the fraction of pores that would have been emptied in a perfectly connected network (F), as illustrated by [21] in Figure 2.0. The mean coordination number, Z, and the number of pore lengths, L, are obtained by fitting the quasi-universal curve of Equation 1.0 to $F(f)$. The mean coordination number of the pore network (Z) is the average number of pores which intersect at a pore junction. The characteristic dimension (L) often refers to typical microparticle size; it maps the linear dimension of the lattices, and thus, it is expressed as a number of pore lengths [21].

Furthermore, during the course of Mercury Porosimetry experiments, batch variability was addressed, and thus, in order to allow for the variation of support structure between pellets of the same batch and to test the reproducibility of measurements, replicate measurements were made for all samples. The reported parameters in this section are the mean of these sets used. After each pressure change, the volume of mercury within the sample was then allowed to come to equilibrium over a period of time. The equilibration time at each of the increasing applied pressures of mercury was set at 50 s. An estimate of the total mercury trapped following depressurization was found from the mercury retraction curve. The entrapped mercury is the difference between the volume at the end of the retraction curve and corresponding pressure point on the intrusion curve (separating interparticle and intraparticle intrusion). Also, the volume of entrapped mercury determines the level of remaining open porosity. The porosity is obtained by taking the ratio of the pore volume and the total volume. It is noteworthy to mention that AutoPore III 9420 mercury porosimeter calculates the solution directly from the raw data.

Tables 2.0 presents the estimated ultimate Mercury entrapment and Pore Connectivity parameters of the investigated materials. The reported uncertainties indicate the spread of the results over samples from the same batch, and the error associated with the technique. The fits of the generalised scaling faction $F(f)$ for one of the samples (Aerosil) is shown in Figure 4.0. It is noteworthy to mention that the connectivity analysis suggested by [21] requires an isotherm where pores are full of condensed nitrogen at the top of the hysteresis loop, thereby corresponding to H1 or H2 hysteresis loop. However, samples such as AL3984T had an incomplete adsorption isotherm due to the limitation of the machine, and thus, still contained vapour in the largest pores that makes the analysis method not applicable. Also, It can be seen in Figure 5.0 that Mercury Entrapment decreases with an increase in pore connectivity.

Table 2
The average result and standard error obtained from nitrogen adsorption isotherms and Mercury Porosimetry of the samples

	Characterization Technique		
	Mercury Porosimetry	Gas Adsorption	
	Entrapment	Connectivity (Z)	Lattice Size (L)
Sample	[%]	[-]	[-]
Aerosil	13.66 ± N/A	6.35 ± 2.65	5.8 ± 0.8
AL3984T	15.51 ± 0.80	6.25 ± 1.75	5.00 ± 1.00
AL3992E	12.23 ± 2.94	N/S	N/S
C10	9.46 ± 1.23	2.00 ± N/A	4.00 ± N/A
C30	3.45 ± 0.23	N/S	N/A
Q17/6	20.26 ± 5.21	2.70 ± 0.3	5.00 ± 1.00
S980A	9.36 ± 0.89	4.30 ± N/A	3.60 ± N/S
S980g	15.18 ± 0.73	N/S	N/S
Silica Alumina	20.69 ± 2.53	N/S	N/S

Note
L - It reflects the aggregate behaviour of microparticles with different shapes and sizes. The microparticles contain pores that are typically in the microscope and mesopore size ranges. Consequently, it is not possible to equate L to any defined dimension, and thus it is regarded as a characteristic dimension of the microparticles [21]
N/A – Not applicable due to lack of sample (Ran out of stock)
N/S – Model not suitable for the set of data

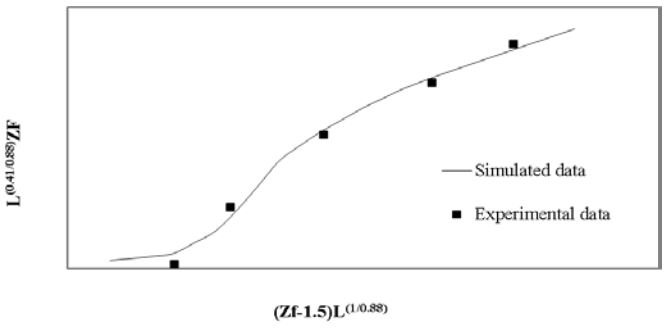

Figure 4.0
Generalised accessibility plot of one of the samples (Aerosil) showing the experiemental and simulated data for $Z = 9$ and $Z = 6.6$

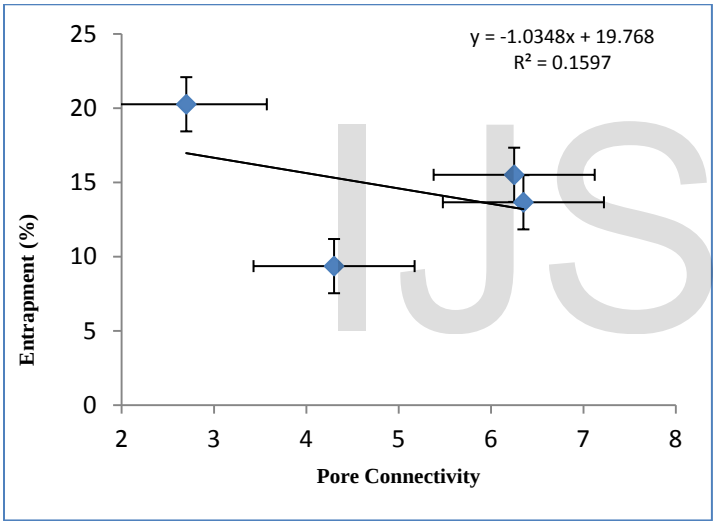

Figure 5.0
Relating the ultimate entrapment with the Pore Connectivity

5.0 DISCUSSION

A novel multi-technique approach has been used to derive structural-topological relationships in order to understand the mechanism of ultimate entrapment in porous materials. As detailed in Section 1.0, several researchers used two and three dimensional bond networks simulation to determine the relationships between structural and transport properties in artificial porous materials. Other workers used basic Corrugated Pore Structure Model (CPSM). Both analytical, basic experimental, and simulation have shown an in increase in Mercury entrapment as tortuosity increases. It in this regard that this section discusses these correlations for structural-topological relationships that were tested with experimental results for a range of porous alumina and silica pellets of spherical or cylindrical geometries.

In general, within the limit of experimental error, for the different pellets studied from the same batch, the isotherms plotted are of type IV classification according to the IUPAC. This is typical of monolayer–multilayer coverage to capillary condensation pattern, with reproducible type H2 hysteresis loops with mesoporous materials. It should be noted that C30 and S980G have type H2 hysteresis loop, however, due to machine limitations; it was not possible to cause the capillary condensation of liquid nitrogen in pores of sizes greater than mesoporosity.

During the course of the mercury porosimetry experiment, the pressure was either increased or decreased in small steps, and thus, this might have affected the pore network of the samples. The high hydraulic pressure applied on materials during intrusion can sometimes lead to partial collapse of the pore network or alteration of the sample during the experiments. Therefore, these pressures may also give rise to potential collapse of the unoccupied pores. Consequently, this will reduce the number of large pores and give false entrapment values [39]. This research has been altered to avoid such limitations, such as the mechanical damage of samples. It is noteworthy to mention that all samples were visually observed after the experiments, to ensure that the high hydraulic pressure applied on the materials did not cause elastic or permanent structural changes. The majority of the test samples retained their external structural stability except for C10, AL3992E, and Silica Alumina. Furthermore, the presence of pore shielding in these materials was previously studied by [15]. It was found that no structural deformation or collapse occurred for these samples.

The mercury entrapment quoted in Table 2.0 was barely affected by the experimental equilibration time, and thus, was considered as the ultimate entrapment. The connectivity characterization method developed by [21] was successfully tested on different sets of materials. As mentioned earlier in this Section, the isotherm plots are of type IV with reproducible type H2 hysteresis loops according to the IUPAC classification. However, some of the samples isotherms were incomplete, and thus, the largest pores still contained vapour at $X = 1$. It is noteworthy to mention that the connectivity characterization method developed by [21] requires an isotherm that has all the characteristics necessary for calculating the PSD by a Kelvin equation based method such as the one suggested by [38]. However, due to machine limitations on achieving relative pressures close to unity, only limited numbers of connectivity parameters were obtained. Also detailed in Section 2.0, [40] showed that the assumption of pore geometry has a significant effect on the mean coordination number (Z). As the exact pore shapes of the samples are unknown, a cylindrical shaped pore model was assumed in this study to align with [21] work. [21] method was particularly robust for Aerosil, AL3984T, C10, Q17/6, and S980A. Similar connectivity parameters were obtained for a range of silica and alumina materials by [21,22,40].

Mercury simulation works, that are detailed in Section 1.0, suggest that mercury entrapment is a function of pore connectivity [5-11]. Similarly [41] stated that for random pore network models of unimodal/monodisperse porous media, simulation results suggest that the mercury entrapment decreased with increased pore connectivity (except for $Z = 2$). These hypothesis was tested on the materials investigated in this study. Therefore, the effect of pore connectivity on mercury entrapment was explored and presented in Figure 5.0. The Mercury entrapment decrease with an increase in Pore Connectivity. To support this correlation, static analysis was carried out in order to rule out any possibility of random chance. A common alpha level for research is 0.10, and was thus adopted in this study [42]. The correlation coefficient obtained for the correlation was 0.1597, and the number of data points used is four. Therefore, by using the critical value table for Pearson's correlation coefficient [42], it can be concluded that the correlation is statistically insignificant. This failure could be attributed to the limitations of the gas sorption technique.

6.0 CONCLUSION

A novel multi-technique approach has been used to predict the relationships between Tortuosity and mercury entrapment. A range of porous alumina and silica pellets of spherical or cylindrical geometries were investigated. In this study, a good statistical correlation was obtained. The Mercury Entrapment decreased with an decreased in Pore Connectivity. However, the correlation is statistically insignificant. The drawback could be attribute to the limitations on the measurement of these pore connectivity descriptors. The standard Method for the characterization of the pore connectivity of porous materials by [21] from gas sorption and percolation theory have been widely used but limited to a selected materials, and thus this paper has expanded the scope of materials used by several researchers in the literature.

ACKNOWLEDGMENT

The authors thanks Professor S.P. Rigby for his valuable discussion in this research.

REFERENCES

[1] Tsakiroglou, C.D., and Payatakes, A.C., 1990. A new simulator of mercury porosimetry for the characterization of porous materials. *Journal of Colloid and Interface Science*, 137, 315-339.

[2] Tsakiroglou C. D., Payatakes A. C., 1998. Mercury Intrusion and Retraction in Model Porous Media, *Adv. Colloid Interf. Sci*., 75, 215–253.

[3] Dullien, F.A.L., 1992. *In porous media; Fluid transport and pore structure*. 2nd edition. New York: Accademic press.

[4] Lowell S., Shields J.E., Thomas, M. A., Thommes, M., 2004. *Characterisation of porous solids and powders; Surface area, pore size and density*. Springer.

[5] Androutsopoulos, G.P. and Mann, R., 1979. Evaluation of mercury porosimeter experiments using a network pore structure model. *Chemical Engineering Science*, 34, 1203-1212.

[6] Washburn, E. W., (1921). The dynamics of capillary flow. *Phys. Rev*., 17, 273-283.

[7] Wardlaw, N.C., McKellar, M., 1981. Mercury porosimetry and the interpretation of pore geometry in sedimentary rocks and artificial models. *Powder Technology*, 29, 127 – 143.

[8] Wardlaw, N.C., 1982. The effects of geometry, wettability, viscosity and interfacial tension on trapping in single pore-throat pairs. *Journal of Canadian Petroleum Technology*, 21, 21-27.

[9] Moscou, L. and S. Lub, 1981. Practical use of mercury porosimetry in the study of porous solids. *Powder Technology*, 29, 45-52.

[10] Portsmouth, R.L., and Gladden, L.F., 1991. Determination of pore connectivity by mercury porosimetry. Chemical Engineering Science, 46 (12), 3023-3036.

[11] Conner, W.C., and Lane, A.M., 1984. Measurement of the morphology of high surface area solids: Effect of network structure on the simulation of porosimetry. *Journal of Catalysis*, 89 (2), 217-225.

[12] Portsmouth, R.L., and Gladden, L.F., 1992. Mercury porosimetry as a probe of pore connectivity. *Chemical Engineering Research and Design*, 70 (1), 63-70.

[13] Rigby, S.P., 2000. A Hierachical Model for the Interpretation of Mercury Porosimetry and Nitrogen Sorption. *J. Colloid and Interface Sci*., 224, 382–396.

[14] Rigby, S.P., and Chigada, P.I., 2009. Interpretation of integrated gas sorption and mercury porosimetry studies of adsorption in disordered networks using mean-field DFT. *Adsorption-journal of the international adsorption society*, 15 (1), 31-41.

[15] Rigby S. P., Fletcher R.S., Riley S. N., 2003b. Determination of the cause of mercury entrapment during porosimetry experiments on sol–gel silica catalyst supports. *Applied Catalysis (A),* 247, 27–39.

[16] Ghaly, G. , Beurroies, I., and Ragai, J., 2010. Mesoporous Titania Gels Prepared from Titanous Chloride and Ammonia: SEM, Nitrogen Adsorption, Thermoporometry and Mercury Porosimetry Studies. Adsorption Science & Technology, Vol. 27 No. 10.

[17] Abell, A., Willis, K., Lange, D., 1999. Mercury intrusion porosimetry and image analysis of cement-based materials. *J Colloid Interface Sci*, 211, 39–44

[18] Ma, H., 2014. Mercury intrusion porosimetry in concrete technology: Tips in measurement, pore structure parameter acquisition and application. *J Porous Mater*. 21:207–215.

[19] Stefan, D., Harald, B., Anna, S., Günter, K., Thomas, R., 2006. Determination of Porosity and Pore Connectivity in Fieldspares from Soils of Granite and Saprolite. Soil Science: 171(9), 675-694.

[20] Turturro, A.C., Caputo, M.C., and Gerke, H.H.,2017. Mercury porosimetry for comparing piece-wise hydraulic properties with full range pore characteristics of soil aggregates and porous rocks. *Geophysical Research Abstracts*, Vol. 19, EGU2017-18729-1.

[21] Seaton, N.A., 1991. Determination of the connectivity of porous solids from nitrogen sorption measurements. *Chemical engineering science*, 46 (8), 1895-1909.

[22] Rigby, S.P., Watt-Smith, M.J., Fletcher, R. S., 2004. Simultaneous determination of the pore-length distribution and pore connectivity for porous catalyst supports using integrated nitrogen sorption and mercury porosimetry. *Journal of catalysis*, 227 (1), 68-76.

[23] Rigby, S.P., Chigada, P.I., Perkins, E.L., Lowe, J., Edler, K.J., 2008. Fundamental studies of gas sorption within mesopores situated amidst inter-connected, irregular network. *Adsorption-journal of the international adsorption society*, 14 (2-3), 289-307.

[24] Ghanbarian, B., Hunt, A.J., Sahimi, M., Ewing, R.P., 2014. Universal Scaling of the formation factor in porous media derived by combining percolation and effective medium theories. *Geophysical Research letters*. Volume 41 (11), 3884-3890.

[25] Broadbent, S.R. and Hammersley, J.M., 1957. Percolation processes, I and II, *Proc. Cambridge Philos. Soc.,* 53, 629.645.

[26] Salmas C.E., and Androutsopoulos, G.P., 2001. A novel pore structure tortuosity concept based on nitrogen sorption hysteresis data. *Industrial engineering chemical research*, 40 (2), 721-730.

[27] Porcheron F., Monson P. A., 2004. Modeling mercury porosimetry using statistical mechanics. *Langmuir*, 20 (15), 6482-6489.

[28] Porcheron F., Monson P. A., 2005. Dynamic aspects of mercury porosimetry: A lattice model study. *Langmuir*, 21, 3179-3186.

[29] Porcheron, F., Monson, P.A., 2005. Molecular modeling of mercury porosimetry. adsorption, *Langmuir*, 11, 325–329.

[30] Vogel, H.J., 1997. Morphological determination of pore connectivity as a function of pore size using serial sections. European Journal of Soil Science, 48, 365–377.

[31] Vogel, H.J., 2000. A numerical experiment on pore size, pore connectivity, water retention, permeability, and solute transport using network models. *European Journal of Soil Science*, 51, 99–105.

[32] Armatas, G.S., and Pomonis, P.J., 2004. A Monte Carlo pore network for the simulation of porous characteristics of functionalized silica: pore size distribution, connectivity distribution and mean tortuosities. *Chemical engineering science*, 59, 5735-5749.

[33] Armatas G.S, Salmas CE, Louloudi M., Androutsopoulos G.P., Pomonis, P.J., 2003. *Relationships among pore size, connectivity, dimensionality of capillary condensation, and pore structure tortuosity of functionalized mesoporous silica.* Langmuir 19 (8), 3128-313.

[34] Armatas, G.S., 2006. Determination of the effects of the pore size distribution and pore connectivity distribution on the pore tortuosity and diffusive transport in model porous networks. *Chemical engineering science*, 61, 4662 – 4675.

[35] Allen, T., 1999. *Particle size measurement*. Dordretch, The Netherlands: Kluwer Academic publishers.

[36] Evbuomwan, O.E., 2009. *The structural characterisation of porous media for use as a model reservoir rocks, adsorbents and catalyst*. Thesis (PhD). University of Bath.

[37] Giesche H., 2006. Mercury porosimetry: A general (practical) overview. *Particle and particles system characterisation*, 23, 9–19.

[38] Barrett, E. P., Joyner, L. G., Halenda, P. P., 1951. The determination of pore volume and area distributions in porous substances. I. Computations from nitrogen isotherms, *J. Am. Chem. Soc*., 73, 373–380.

[39] Pirard R., Heinrichs B., Pirard J.P. in: McEnaney B., Mays T.J., Rouquerol J., Reinoso R.F., Sing K.S.W., Unger (Eds.) K.K., 1997. *Characterisation of Porous Solids IV, Royal Society of Chemistry*. Cambridge.

[40] Liu, H., Zhang, L., Seaton, N.A., 1992. Determination of the connectivity of porous solids from nitrogen sorption measurements-II. Generalisation. *Chemical Engineering Science*, 47(17-18), 4393-4404.

[41] Friedman, S.P., Zhang L., Seaton, N.A., 1995. Gas and Solute Diffusion Coefficients in Pore Networks and its Description by a Simple Capillary Model. *Transport in Porous Media*, 19 (3), 281-301.

[42] Chatfield, C., 1983. *Statistics for technology: A course in applied statistics*. Chapman & Hall/CRC.